A&A 428, 867–875 (2004)
DOI: 10.1051/0004-6361:20041426

Astronomy & Astrophysics

RX J1821.6+6827: A cool cluster at $z = 0.81$ from the *ROSAT* NEP survey⋆

I. M. Gioia[1,⋆⋆,⋆⋆⋆], A. Wolter[2], C. R. Mullis[3,⋆⋆,⋆⋆⋆], J. P. Henry[4,⋆⋆⋆], H. Böhringer[5], and U. G. Briel[5]

[1] Istituto di Radioastronomia CNR, via P. Gobetti 101, 40129 Bologna, Italy
e-mail: gioia@ira.cnr.it
[2] INAF – Osservatorio Astronomico di Brera, via Brera 28, 20121 Milano, Italy
e-mail: anna@brera.mi.astro.it
[3] European Southern Observatory, Karl-Schwarzschild-Str. 2, Garching bei München 85740, Germany
e-mail: cmullis@eso.org
[4] Institute for Astronomy, 2680 Woodlawn Drive, Honolulu, HI 96822, USA
e-mail: henry@ifa.hawaii.edu
[5] Max-Planck-Institut fur Extraterrestrische Physik, Giessenbachstrasse, Postfach 1312, Garching 85741, Germany
e-mail: hxb@xray.mpe.mpg.de,ugb@xray.mpe.mpg.de

Received 7 June 2004 / Accepted 30 July 2004

Abstract. We present an analysis of the properties of the cluster of galaxies RX J1821.6+6827, or NEP 5281, at a redshift $z = 0.816 \pm 0.001$. RX J1821.6+6827 was discovered during the optical identification of the X-ray sources in the North Ecliptic Pole (NEP) region of the *ROSAT* All-Sky Survey and it is the highest redshift cluster of galaxies of the NEP survey. We have measured spectroscopic redshifts for twenty cluster galaxies using the Keck-I and the Canada-France-Hawai'i (CFH) telescopes. The value for the cluster velocity dispersion is $\sigma_V = 775^{+182}_{-113}$ km s^{-1}. The cluster was also observed by XMM-*Newton*. Both the optical and X-ray data are presented in this paper. The cluster has an unabsorbed X-ray flux in the 2−10 keV energy band of $F_{2-10\ \mathrm{keV}} = 1.24^{+0.16}_{-0.23} \times 10^{-13}$ erg cm^{-2} s^{-1} and a K-corrected luminosity in the same band of $L_{2-10\ \mathrm{keV}} = 6.32^{+0.76}_{-0.73} \times 10^{44}\ h_{50}^{-2}$ erg s^{-1} (90% confidence level). The cluster X-ray bolometric luminosity is $L_{\mathrm{BOL,X}} = 1.35^{+0.08}_{-0.21} \times 10^{45}\ h_{50}^{-2}$ erg s^{-1} ($L_{\mathrm{BOL,X}} = 1.17^{+0.13}_{-0.18} \times 10^{45}\ h_{70}^{-2}$ erg s^{-1} in the concordance cosmology). The data do not allow fitting both metal abundance and temperature at the same time. The abundance is unconstrained and can vary in the range $0.28-1.42\ Z_\odot$ while the best fit X-ray temperature is $T = 4.7^{+1.2}_{-0.7}$ keV. This emission weighted X-ray temperature is a little lower, barely within the uncertainties, than the predicted temperature, $T = 6.34^{+0.13}_{-0.35}$ keV, from the $L_X - T_X$ relation of local clusters published in the literature. The optically measured velocity dispersion is consistent with the velocity dispersion expected from the $\sigma_V - T_X$ relationship. We also examine the point X-ray source RX J1821.9+6818, or NEP 5330, located to the south east of the cluster which was identified as a QSO at $z = 1.692 \pm 0.008$ in the *ROSAT* NEP survey. The X-ray source is well fitted by an absorbed power law model with $N_H = 4.1^{+3.1}_{-3.0} \times 10^{20}$ atoms cm^{-2} and a photon index $\Gamma = 1.67 \pm 0.12$ typical of an active galactic nucleus.

Key words. galaxies: clusters: general – galaxies: clusters: individual: RX J1821.6+6827 – X-rays: general – X-rays: individuals: RX J1821.6+6827 – X-rays: galaxies: clusters – galaxies: intergalactic medium

1. Introduction

Clusters of galaxies are the most massive, collapsed structures in the Universe. They are the highest peaks in a cosmic terrain driven by gravitational clustering and represent the manifestations of cosmic structure building (Peebles 1993; Peacock 1999). The study of the properties of clusters at intermediate and high redshift, both individually and as a population, is important since it allows different cosmological and structure formation models to be tested and constrained. The internal mix of components within clusters, as well as the space density of the most distant and massive clusters and the temperature distribution function of X-ray clusters, can be used to determine fundamental cosmological parameters (Henry & Arnaud 1991; Oukbir & Blanchard 1992, 1997; Eke et al. 1998; Borgani et al. 1999, 2001; Henry 2000, 2004; Vikhlinin et al. 2003). Through the detection of X-ray emission from the hot

⋆ Data presented here used the XMM-*Newton* facility.
⋆⋆ Visiting Astronomer at the W. M. Keck Observatory, jointly operated by the California Institute of Technology, the University of California and the National Aeronautics and Space Administration.
⋆⋆⋆ Visiting Astronomer at the Canada-France-Hawai'i Telescope, operated by the National Research Council of Canada, le Centre National de la Recherche Scientifique de France and the University of Hawai'i.

intracluster gas, X-ray cluster surveys are unbiased in the sense that they exclusively select gravitationally bound objects and are essentially unaffected by projection effects. There are only a few known clusters of galaxies beyond redshift unity, most of them were found in X-ray survey samples (see Rosati et al. 2004). Even if we are far from having very large complete samples of distant ($z > 0.8$) clusters, our capabilities to discover and observe distant objects are rapidly increasing as more accurate and sensitive observing techniques become available.

In recent years we have been involved in the study of the deepest region of the *ROSAT* All-Sky Survey, at the North Ecliptic Pole (Henry et al. 2001; Voges et al. 2001), to produce a complete and unbiased X-ray-selected sample of clusters of galaxies. The resulting NEP cluster sample has been used to investigate the nature of cluster evolution (Gioia et al. 2001) and to explore the potential implications for large-scale structure models (Mullis et al. 2001). RX J1821.6+6827, or NEP 5281, was detectd in the *ROSAT* NEP survey as a 4.5σ source with only 40 ± 9 net photons in a vignetting corrected exposure of 5519 s. The identification program of the survey (Gioia et al. 2003) revealed the cluster nature of the source. Optical spectroscopic observations with the CFH and Keck-I telescopes placed the cluster at a redshift of $z = 0.816 \pm 0.001$. RXJ 1716.6+6708 is the most distant cluster of galaxies in the *ROSAT* NEP survey. Follow-up XMM-*Newton* observations were also performed, and are reported here together with the optical observations. Note that this is the second $z = 0.81$ cluster discovered in the NEP survey. The first one, RXJ 1716.6+6708 (Gioia et al. 1999), does not appear in the final complete NEP sample because it did not meet the selection criterium for source count rate of signal-to-noise ratio $\geq 4\sigma$.

Section 2 describes the optical and X-ray data acquisition and analysis. Section 3 details the results obtained and discuss these results. A brief summary is given in Sect. 4. Throughout this paper, we assume an Einstein-de Sitter model $H_0 = 50\ \mathrm{km\,s^{-1}\,Mpc^{-1}}$, $\Omega_\mathrm{M} = 1$, and $\Omega_\Lambda = 0$ for direct comparison to previous work in this field, but we also repeat the calculations in the current cosmological concordance model $(h, \Omega_\mathrm{M}, \Omega_\Lambda) = (0.7, 0.3, 0.7)$. At the redshift of the cluster, the luminosity distance is 5.62 h_{50}^{-1} Gpc, the angular size distance is 1.70 h_{50}^{-1} Gpc, and the scale is 8.26 h_{50}^{-1} kpc per arcsec. Throughout the paper quoted uncertainties are 90% confidence levels for one interesting parameter.

2. Observations and data analysis

In this section we present the optical spectroscopy for the cluster galaxies performed at the CFHT and Keck-I and the X-ray follow-up observations of RX J1821.6+6827 acquired with XMM-*Newton*. We first describe the optical spectroscopy, and then present the X-ray data which show that NEP 5281 has a low temperature, lower than expected from its bolometric luminosity, but commensurate with its velocity dispersion. We also present the optical and X-ray data on the point source to the south east of the cluster, namely RX J1821.9+6818, or NEP 5330, which is identified with a QSO at $z = 1.692$.

2.1. CFHT and Keck-I spectroscopy

RX J1821.6+6827 was observed on July 3, 1997, at the CFHT with the MOS instrument using the STIS2 2048^2 and the O300 grism in multislit mode. The wavelength coverage was from 4000 to 10 000 Å and the pixel size was 4.8 Å $\mathrm{pix^{-1}}$. The slitlet width of 1.5″ provided a spectral resolution of 17 Å. The data were reduced using the MULTIRED package developed by Le Fevre et al. (1995). Seven galaxies from the CFHT data were identified as cluster members from the CaII break only (one has [OII] in emission). NEP 5281 was also observed at the Keck-I telescope on June 22, 2001, with the Low Resolution and Imaging Spectrograph (LRIS, Oke et al. 1995) in slitmask mode. With both spectrographs in operation, LRIS_R and LRIS_B, it is possible to obtain multi-object spectra covering the entire optical window in one integration. However we used only data from the red arm given the redshift of the cluster. The 600 l/mm grating blazed at 7850 Å, to target [OII] plus Ca II break and CN at the redshift of the cluster. Combined with our grating angle the wavelength coverage was approximately 6500 Å to 9500 Å, and the pixel size was 1.25 Å. The GG495 filter was used to eliminate the overlapping second order spectrum to avoid any contamination blueward of 9500 Å. Given the fact that galaxies are extended objects, even at this redshift, we used a slit width of 1.4″, which gives a spectral resolution of roughly 6.5 Å. For the selection of the objects to spectroscopically observe, we used deep two color (B and I) images previously taken by us at the University of Hawai'i (UH) 2.2 m telescope. The UCSCLRIS package designed by Drew Phillips and collaborators at Lick Observatory was used to prepare the slit-mask files. We designed two masks at different position angles in order to cover the central part of the cluster. Only data from the first slitmask were used since the second slitmask exposure was affected by heavy cirrus and bad weather. Thus we do not have a complete coverage for the galaxies in the central region of the cluster. The first mask was exposed for 10 800 s. After the mask exposure, flat fields and arc calibrations exposures were also obtained. The data have been reduced using the standard IRAF package routines for 2D spectra images. The two-dimensional spectra had to be straightned using the software package WMKOLRIS kindly provided by Greg Wirth at the W. M. Keck Observatory.

Fifteen galaxies out of 26 observed objects were recognized as cluster members on the basis of CaII H and K, CN and, in some cases, the G band absorption features. Only one of the 15 galaxies observed had [OII] in emission. Two of the seven galaxies observed at the CFHT are common to the Keck-I observations. In the end, 15 unique objects observed by Keck plus 5 unique objects observed by CFHT turned out to be cluster member galaxies. These twenty galaxies are listed in Table 1. For each galaxy the (J2000) coordinates, measured velocity, 1σ error, and redshift are given. In the last column the main spectral features are also noted.

The velocity histogram for the 20 member galaxies is shown in Fig. 1. There is a low-velocity extension in the histogram at 238 500 $\mathrm{km\,s^{-1}}$ (2 galaxies) that our 3σ iterative clipping algorithm (following Danese et al. 1980) excludes from the computation of the cluster velocity. From 18 accepted

Table 1. Spectroscopic data for the galaxies in the NEP cluster RX J1821.6+6827.

ID	RA (J2000)	Dec (J2000)	cz	Δcz	z	Spectral features
#	h m s	° ′ ″	km s^{-1}	km s^{-1}		
1	18 21 16.6	+68 30 25	244 367	120	0.8151	$H+K$, G band, $H\delta$, CN
2	18 21 21.5	+68 29 57	246 585	240	0.8225	$H+K$, CN
3	18 21 26.2	+68 29 31	246 016	170	0.8206	$H+K$, G band, CN
4	18 21 30.8	+68 29 29	245 856	180	0.8204	$H+K$, G band, CN
5	18 21 27.9	+68 28 43	246 705	480	0.8229	$H+K$, G band, CN
6	18 21 33.8	+68 28 40	246 885	210	0.8235	$H+K$
7	18 21 32.6	+68 27 54	244 847	180	0.8167	$H+K$, G band, cD ?
8	18 21 34.9	+68 27 53	242 808	90	0.8099	$H+K$, CN
9	18 21 37.2	+68 27 51	244 428	389	0.8153	$H+K$ G band, CN
10	18 21 33.6	+68 27 50	243 317	389	0.8161	$H+K$, G band
11	18 21 35.2	+68 27 34	243 288	60	0.8115	$H+K$, CN
12	18 21 36.6	+68 27 21	244 996	120	0.8172	$H+K$
13	18 21 37.5	+68 27 07	246 765	150	0.8231	$H+K$
14	18 21 37.9	+68 27 00	244 607	60	0.8159	$H+K$
15	18 21 18.2	+68 27 00	238 102	840	0.7942	[OII]
16	18 21 47.7	+68 27 06	242 508	30	0.8089	$H+K$
17	18 21 51.1	+68 27 17	241 639	540	0.8060	CaII Break
18	18 21 57.7	+68 27 25	243 378	540	0.8118	CaII Break
19	18 21 50.8	+68 26 09	244 397	840	0.8152	CaII Break, [OII]
20	18 21 47.8	+68 25 18	243 498	90	0.8122	$H+K$

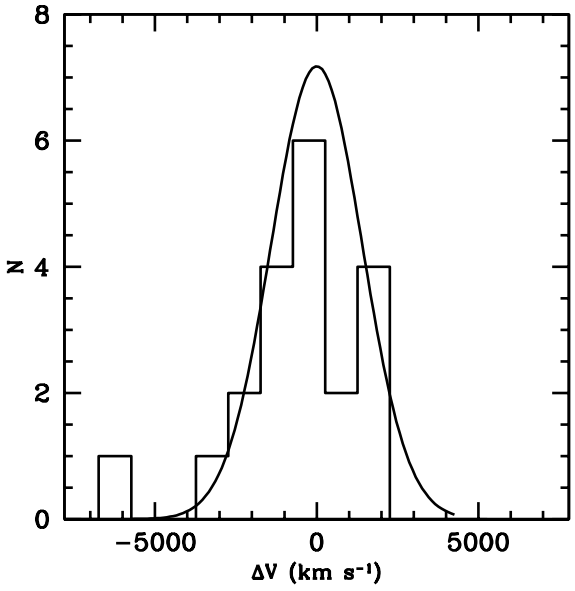

Fig. 1. Distribution of velocities for the 20 galaxies showing a low velocity tail at $\Delta_v \sim -6000$ km s^{-1}. The curve shows a Gaussian distribution centered at $\langle v \rangle = 244\,736$ km s^{-1} with width given by the derived $\sigma_V = 1407$ km s^{-1} (not corrected to the first order for cosmological redshift) and normalized for the 18 galaxies considered as cluster members.

cluster members, and taking into account the errors on the redshift, we obtain a mean velocity $\langle v \rangle = 244\,736 \pm 325$ km s^{-1}, an average redshift $\langle z \rangle = 0.8163 \pm 0.0011$, and a dispersion along the line of sight $\sigma_V = 775^{+182}_{-113}$ km s^{-1} (corrected to first order for cosmological redshift by dividing by $1+z$). Without the 3σ clipping the mean velocity for the 20 galaxies is $\langle v \rangle = 244\,249 \pm 384$ km s^{-1}, the average redshift is $\langle z \rangle = 0.8148 \pm 0.0016$, and the dispersion along the line of sight is $\sigma_V = 1142^{+247}_{-155}$ km s^{-1}.

Using the ROSTAT software by Tim Beers and collaborators (Beers et al. 1990) (see also Bird & Beers 1993) we obtain very similar results to those of the 3σ iterative clipping algorithm by Danese et al. (1980). Below the values obtained by the biweight estimator of scale, as suggested by Beers et al. (1990) for this number of galaxies, are given. The errors are the 90% confidence intervals. The average redshift is $\langle z \rangle = 0.8156 \pm 0.0024$ accounting for errors on z ($\langle z \rangle = 0.8147 \pm 0.0044$ with no errors), and a $\sigma_V = 577 \pm 231$ km s^{-1}, corrected to first order for cosmological redshift ($\sigma_V = 1048 \pm 421$ km s^{-1} corrected to first order cosmological redshift but without taking into account the errors on redshift), which are consistent with either the 20 cluster member and the 18 cluster member velocity dispersions obtained with the previously adopted 3σ clipping algorithm.

2.2. XMM-Newton observations

XMM-*Newton* (Jansen et al. 2001) observed RX J1821.6+6827 as part of the GO program in three epochs, on November 13 and 23, 2002, and on December 19, 2002, for a nominal exposure of 63 Ks with the European Photon Imaging Camera (EPIC) pn (Strüder et al. 2001) and for 73.5 ks with the

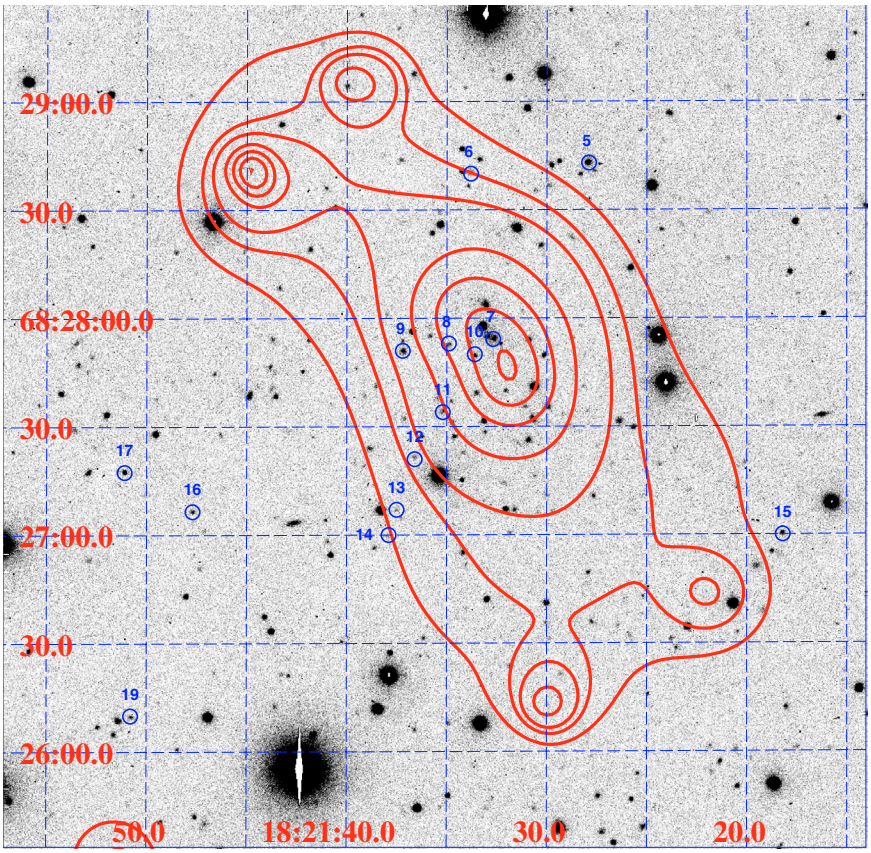

Fig. 2. 1800 s *I*-band image of RX J1821.6+6827 taken at the UH 2.2 m telescope. The combined MOS1 and MOS2 image was smoothed with a Gaussian to have 16 pixels per cell (corresponding to 8″). The energy range is 0.3–8 keV band. Units for the smoothed overlayed X-ray contours are (6.5, 7.8, 9.1, 13, 18.2, 24.7, 32.5) $\times 10^{-3}$ counts s^{-1} arcmin^{-2} over the background which correspond to (2.5, 3, 3.5, 5, 7, 9.5, 12.5)σ over the background. The circles indicate 14 out of 20 cluster members. The cD galaxy is marked as galaxy # 7. The other 6 galaxies at the redshift of the cluster fall outside the field of view (see Table 1). The image measures 1092 × 1092 pixels covering a field of 4′ × 4′ (1.98 h_{50}^{-1} × 1.98 h_{50}^{-1} Mpc at $z = 0.8163$).

EPIC MOS CCD arrays (Turner et al. 2001). The pn was operating in extended-full-frame mode with thin filter while the MOS was in the full-frame mode also with the thin filter applied. The pileup is not a problem given the low count rate of the X-ray source.

Unfortunately the observations suffer from periods of very high background. Event files produced by the standard pipeline processing have been examined and filtered to remove the high background time intervals (using the version 5.4.1 of the Science Analysis Software, SAS, and the latest calibration files released by the EPIC team). Only events corresponding to pattern 0–12 for MOS and pattern 0–4 for pn have been used[1]. Good time intervals were selected by applying thresholds of 0.35 counts s^{-1} in the MOS and 1 counts s^{-1} in the pn to the photons at energies greater than 10 keV. At these higher energies counts come mostly from background. The net exposure times, after data cleaning, are 21.3 Ks and 22.0 Ks for the MOS 1 and MOS 2, respectively, and 10.6 Ks for the pn. For subsequent analysis background counts have been accumulated using nearby source-free circular regions.

The three images, one for each instrument, taken on different epochs were summed using the SAS task *merge*. Given the position of the source at the center of the field, the different orientations of the instrument with respect to the sky coordinates should not affect the response of the instruments. Thus resulting response matrices and auxiliary files are the average of the three exposures, weighted by the different exposure times.

Response matrices (that include the correction for the effective area) have been generated using the SAS tasks *arfgen* and *rmfgen*. The X-ray fluxes reported below are computed using the MOS1 detector and calibration(s). From our data the normalization of the MOS2 is 5% lower than that of the MOS1 whereas the normalization of the pn is 24% lower. This apparently discrepant normalization value has to be attributed to the fact that the cluster falls on the CCD gap of the pn.

2.3. Overall cluster properties

Figure 2 shows the XMM-*Newton* smoothed contours of RX J1821.6+6827 overlayed onto an optical 1800 s *I* band image taken at the UH 2.2 m telescope. Both MOS1 and MOS2

[1] See the XMM-*Newton* Users' Handbook
http://xmm.vilspa.esa.es/external/xmm_user_support/documentation/uhb/XMM_UHB.htm

Table 2. X-ray properties of RX J1821.6+6827 (NEP 5281) and RX J1821.9+6818 (NEP 5330).

RA (J2000)	Dec (J2000)	Instr	R	Net Cts	T	Z ($Z_\odot$)	N_H	Region
h m s	° ′ ″		″		keV	Γ	$\times 10^{20}$ at/cm^2	
18 21 32.5	+68 27 45.0				$4.7^{+1.2}_{-0.7}$	$0.77^{+0.65}_{-0.49}$	frozen[a]	cluster
		MOS1	100	708 ± 35				
		MOS2	100	671 ± 36				
		pn	100	751 ± 40				
18 21 58.3	+68 18 41.2					1.67 ± 0.12	$4.1^{+3.1}_{-3.0}$	QSO
		MOS1	25	609 ± 25				
		MOS2	25	632 ± 26				
		pn	25	874 ± 30				

[a] N_H fixed at the Galactic value of 5.24×10^{20} atoms cm^{-2}.

data were used to produce the X-ray contours in the 0.3−8 keV band. The data were smoothed with a Gaussian using cells of 16 pixels corresponding to a resolution of 8″. The X-ray cluster is extended along the NE–SW direction. There are not enough X-ray counts to produce a more meaningful comparison between the optical and X-ray images.

To measure the emission-weighted cluster temperature, net counts were extracted from a circle of radius 100″ centered at $\alpha_{2000} = 18^h21^m32.5^s$, $\delta_{2000} = +68°27'45.0''$ which corresponds to the barycenter of the X-ray emission and is very close to the position of galaxy 7 (see Table 1). At the redshift of the cluster such a radius corresponds to a linear size of 826 h_{50}^{-1} kpc. A larger radius including more extended emission counts could not be chosen given the high increment in background counts. There are 708 ± 35 net counts in the (0.4−4.0 keV) energy range in the MOS1 detector, 671 ± 36 in (0.5−4.3 keV) in the MOS2, and 751 ± 40 net counts in (0.5−3.4 keV) in the pn detector. X-ray properties are listed given in Table 2. The data were fitted in XSPEC (version 11.3.0) with a single temperature MEKAL model (Mewe et al. 1985) modified by Galactic absorption, where the ratio between the elements are fixed to the solar values as in Anders & Grevesse (1989)[2].

The relative normalization of the three instruments was left free to account for possible intercalibration differences or mismatches. The absorption and redshift were kept constant while the temperature and abundance were left free to vary. The absorption was fixed at the Galactic value of 5.24×10^{20} atoms cm^{-2} (Elvis et al. 1994) and the redshift was fixed at $z = 0.8163$. The best fit with a thermal MEKAL model gives a temperature $T = 4.7^{+1.2}_{-0.7}$ keV and a best fit abundance $Z = 0.77\ Z_\odot$, which is unconstrained by these data due to a non-detection of the iron K line. The metallicity can vary in the range 0.28–1.42 $Z_\odot$. The binned X-ray spectrum and best fit folded model are shown in Fig. 3 where bins were chosen so as to have each resulting energy channel significant at the signal-to-noise ratio of at least 4. The total number of photons in each

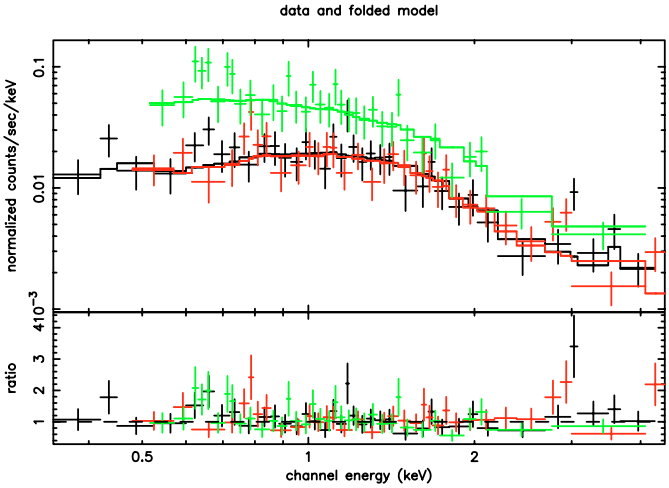

Fig. 3. Binned X-ray spectrum and residuals for RX J1821.6+6827. The spectrum was binned in such a way that each resulting energy channel has a signal-to-noise ratio of at least 4. The solid line represents the best fit MEKAL model. The top grey spectrum is the pn spectrum, while the lower and darker spectra are the MOS1 and MOS2 spectra.

bin allows the use of the χ^2 statistics for the fit. The fit has a reduced χ^2 of 0.90 for 102 degrees of freedom. If one fixes the abundance to $Z = 0.5\ Z_\odot$ then the temperature increases a little ($T = 4.9^{+1.2}_{-0.8}$ kev) but it is consistent with the previously determined temperature within the errors. The reduced χ^2 becomes 0.90 for 103 degrees of freedom.

The unabsorbed flux in the 2−10 keV energy band is $F_{2-10\ \mathrm{keV}} = 1.24^{+0.16}_{-0.23} \times 10^{-13}$ erg cm^{-2} s^{-1}, (see Table 3). While the unabsorbed X-ray flux in 0.5−2.0 keV band is $F_{0.5-2.0\ \mathrm{keV}} = 1.35^{+0.13}_{-0.21} \times 10^{-13}$ erg cm^{-2} s^{-1}, to be compared with the flux obtained with the *ROSAT* PSPC in 0.5−2.0 keV of $F_{\mathrm{X,ROSAT}} = 1.02 \pm 0.22 \times 10^{-13}$ erg cm^{-2} s^{-1}. The K-corrected luminosity in the 2−10 keV energy band is $L_{2-10\ \mathrm{keV}} = 6.32^{+0.76}_{-0.73} \times 10^{44}\ h_{50}^{-2}$ erg s^{-1} while the bolometric luminosity is $L_{\mathrm{BOL,X}} = 1.35^{+0.08}_{-0.21} \times 10^{45}\ h_{50}^{-2}$ erg s^{-1}. The luminosity in the 0.5–2.0 keV obtained with XMM-*Newton* is $L_{0.5-2.0\ \mathrm{keV}} = 4.04^{+0.47}_{-0.58} \times 10^{44}\ h_{50}^{-2}$ erg s^{-1}, comparable with the *ROSAT* PSPC luminosity

[2] These values for the solar metallicity have recently been superseded by the new values of Grevesse & Sauval (1998), who used a 0.676 times lower Fe solar abundance. However, we prefer to report metallicities in the units of Anders & Grevesse abundances since most of the literature still refers to these old values.

Table 3. Fluxes and luminosities for the galaxy cluster and the QSO.

RA (J2000)	Dec (J2000)	$F_{2-10\ \mathrm{keV}}$	z	$L_{2-10\ \mathrm{keV}}$	L_{BOL}	Region
h m s	° ′ ″	10^{-13} cgs		$10^{44}\ h_{50}^{-2}$ cgs[a]	$10^{45}\ h_{50}^{-2}$ cgs	
				$10^{44}\ h_{70}^{-2}$ cgs[a]	$10^{45}\ h_{70}^{-2}$ cgs	
18 21 32.5	+68 27 45.0	$1.24^{+0.16}_{-0.23}$	0.816 ± 0.001	$6.32^{+0.76}_{-0.73}$	$1.35^{+0.08}_{-0.21}$	cluster
				$5.48^{+0.56}_{-0.74}$	$1.17^{+0.13}_{-0.18}$	
18 21 58.3	+68 18 41.2	3.66 ± 0.39	1.692 ± 0.008	50^{+5}_{-7}		QSO
				53^{+6}_{-5}		

[a] First line refers to the Einstein-de-Sitter model with $H_0 = 50\ \mathrm{km\,s^{-1}\,Mpc^{-1}}$, $\Omega_{\mathrm{M}} = 1$, and $\Omega_\Lambda = 0$, while second line refers to the cosmological concordance model with $H_0 = 70\ \mathrm{km\,s^{-1}\,Mpc^{-1}}$, $\Omega_{\mathrm{M}} = 0.3$, $\Omega_\Lambda = 0.7$.

of $L_{\mathrm{X,ROSAT}} = (2.91 \pm 0.63) \times 10^{44}\ h_{50}^{-2}\ \mathrm{erg\,s^{-1}}$. In the concordance cosmology the K-corrected luminosity in the 2−10 keV energy band becomes $L_{2-10\ \mathrm{keV}} = 5.48^{+0.56}_{-0.74} \times 10^{44}\ h_{70}^{-2}\ \mathrm{erg\,s^{-1}}$ and the bolometric luminosity becomes $L_{\mathrm{BOL,X}} = 1.17^{+0.13}_{-0.18} \times 10^{45}\ h_{70}^{-2}\ \mathrm{erg\,s^{-1}}$.

As can be seen from Fig. 2 there are point-like sources both to the north-east and the south-west which are included in the 100″ radius even if it is unclear if they belong to the cluster. The data were re-analyzed excluding the point sources from the measure of the cluster X-ray temperature. Freezing as before the Galactic absorption to the neutral hydrogen column density $N_{\mathrm{H}} = 5.24 \times 10^{20}$ atoms cm^{-2}, the redshift to $z = 0.8163$ and leaving the abundance free to vary, a value of $T = 4.9^{+1.6}_{-0.9}$ keV is determined for the cluster gas once the point sources are excluded. The fit has a reduced χ^2 of 0.91 for 85 degrees of freedom. This value for the temperature is perfectly consistent with the temperature previously obtained ($T = 4.7^{+1.2}_{-0.7}$ keV) within the uncertainties.

2.4. RX J1821.9+6818, or NEP 5330: the QSO at z = 1.692 in the XMM-Newton field

There are at least 20 point sources in the XMM-*Newton* image. We discuss here only one point source, RX J1821.9+6818, which appears in the NEP survey catalog (Gioia et al. 2003) as NEP 5330, and which is not visible in Fig. 2 since it is outside the field of view. The source was identified with an AGN1 (or type 1 AGN, a classification which includes either Seyfert 1 and QSO objects) at redshift $z = 1.692 \pm 0.008$. The object was spectroscopically observed at the UH 2.2 m telescope as part of the identification program of the NEP survey sources on June 18, 1998. The telescope was equipped with the Wide Field Grism Spectrograph and the Tek2048 CCD. We used the 420 l mm^{-1} red grism and a 300 μ slit (2.4″) which provided at the $f/10$ focus a pixel scale in spectroscopic mode of 3.6 Å pix^{-1}, a spectral resolution of ∼19 Å *FWHM*, and a wavelength coverage of approximately 3900 Å–9500 Å.

The classification with an AGN1 has been done on the basis of the equivalent width of the emission lines ($W_\lambda \sim 30$ Å) and on the *FWHM* (∼4000 km s^{-1}) of the broad permitted emission

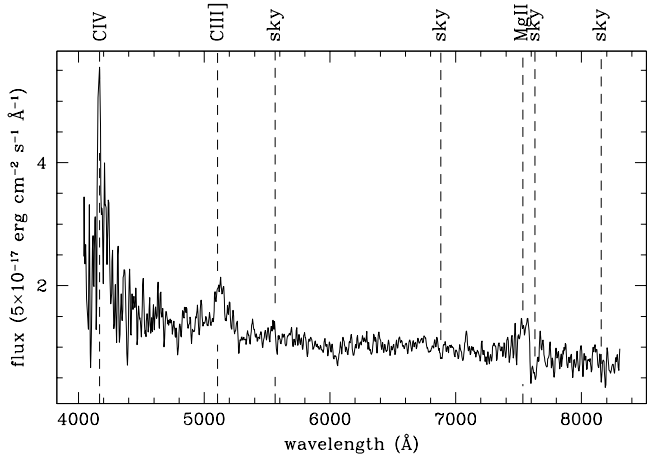

Fig. 4. Long-slit spectrum taken at the UH 2.2 m of the QSO at $z = 1.692$ associated to RX J1821.9+6818. The total integration time was of 2400 s. The dashed lines indicate the positions of the CIV, CIII], Mg emission lines at the QSO redshift. Wavelengths of atmospheric absorption bands are also indicated.

lines, indicating a QSO type object (see Gioia et al. 2003 for more details on the optical classification). An optical spectrum is shown in Fig. 4 where the dashed lines indicate the positions of the emission lines at the QSO redshift. Wavelenghts of atmosphric absorption bands are also indicated.

To examine the X-ray source associated to the QSO, a circle of radius 25″ was centered at $\alpha_{2000} = 18^{\mathrm{h}}21^{\mathrm{m}}58.3^{\mathrm{s}}$, $\delta_{2000} = +68°18'41.2''$. There are a total of 609 ± 25 net counts in the (0.4−3.8 keV) energy range in the MOS1 detector, 632 ± 26 in (0.5−4.6 keV) in the MOS2, and 874 ± 30 net counts in (0.5−6.2 keV) in the pn detector (see Table 2). The data were fitted in XSPEC with an absorbed power law model given the nature of the source. The relative normalization of the three instruments was left free. The X-ray flux reported below is computed using the MOS1 detector and calibration. The normalization of the MOS2 is 2% lower than that of the MOS1 whereas the normalization of the pn is 3% lower. The three instrument normalizations are in better agreement than in the analysis of the cluster source implying that the high normalization

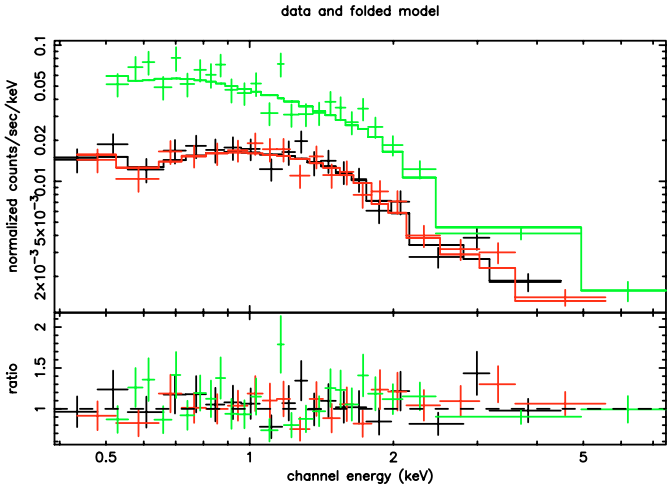

Fig. 5. Binned X-ray spectrum and residuals for RX J1821.9+6818, the QSO in the XMM-*Newton* field. The spectrum was binned in such a way that each resulting energy channel has a signal-to-noise ratio of at least 5. The solid line represents the best fit power law model. The top grey spectrum is the pn spectrum, the MOS1 and MOS2 spectra are the two lower and darker spectra.

discrepancy (24%) found previously for the pn with respect to the two MOS detectors is most probably due to the fact that the cluster falls in one of the gap of the pn.

Both the absorption and the photon index (Γ) of the power law model were free to vary. The best fit Γ is 1.67 ± 0.12 and the best fit absorption is $N_{\rm H} = 4.1^{+3.1}_{-3.0} \times 10^{20}$ atoms cm^{-2}, consistent with the Galactic value of $N_{\rm H} = 5.24 \times 10^{20}$ atoms cm^{-2}. The binned X-ray spectrum and best fit folded model are shown in Fig. 5 where bins were chosen so as to have each resulting energy channel significant at the signal-to-noise ratio of at least 5. The fit has a reduced χ^2 of 0.92 for 61 degrees of freedom. The unabsorbed flux of the QSO in the 2−10 keV energy band is $F_{2-10\ \rm keV} = (3.66 \pm 0.39) \times 10^{-13}$ erg cm^{-2} s^{-1} (see Table 3). The K-corrected luminosity in the 2−10 keV energy band is $L_{2-10\ \rm keV} = 5.0^{+0.5}_{-0.7} \times 10^{45}\ h_{50}^{-2}$ erg s^{-1}. In the concordance cosmology the K-corrected luminosity in the 2−10 keV energy band becomes $L_{2-10\ \rm keV} = (5.3^{+0.6}_{-0.5}) \times 10^{45}\ h_{70}^{-2}$ erg s^{-1}. Note that the luminosity of RX J1821.9+6818 as measured with XMM-*Newton* in 2002 is approximately 2.5 times higher than that measured with ROSAT in 1990 (see Mullis et al. 2004 for revised fluxes and luminosities for NEP AGN). Such a difference is not surprising given the time variability of AGN.

RX J1821.9+6818 was also observed with the Very Large Array at 1.5 GHz by Kollgaard et al. (1994) who mapped a 29.3 deg^2 region surrounding the north ecliptic pole to support the deepest portion of the *ROSAT* all-sky soft X-ray survey. RX J1821.9+6818 was detected by the the VLA-NEP survey with a flux density of 182 mJy at 1.5 GHz.

3. Discussion and conclusions

The main result of this paper is the presentation of the optical and X-ray data, namely the spectroscopic data acquired through Keck-I, CFH and UH 2.2 m telescopes, and the X-ray temperature obtained with the detectors onboard the XMM-*Newton* satellite. We will focus the following discussion on the implications of measured quantities such as the emission weighted temperature and velocity dispersion for RX J1821.6+6827. As with other X-ray selected, distant clusters RX J1821.6+6827 does not have a spherically symmetric morphology in X-rays or in optical. Its X-ray morphology is elongated and very similar to other ∼0.8 clusters like RXJ 1716.6+6708 (Gioia et al. 1999), another cluster found in the course of the NEP identification program but which did not meet the 4σ selection criterium for sources (Gioia et al. 2003), or to the better known Medium Survey cluster MS 1054−0321 (Gioia et al. 2004). Differently from RXJ 1716.6+6708 and MS 1054−0321 that both show high velocity dispersions ($\sigma_{\rm V} = 1522^{+215}_{-150}$ km s^{-1} and $\sigma_{\rm V} = 1150 \pm 97$ km s^{-1}, respectively: Gioia et al. 1999; van Dokkum et al. 2000), RX J1821.6+6827 has a velocity dispersion of $\sigma_{\rm V} = 775^{+182}_{-113}$ km s^{-1}, rather typical of normal relaxed clusters. We are also dealing with a cool cluster with a temperature ($T = 4.7$ keV) a little lower than the temperature of RXJ 1716.6+6708 (which *Chandra* measured to be $T = 6.6 \pm 0.8$ keV; Vikhlinin et al. 2002) and even lower than the X-ray temperature of MS 1054−0321 (which XMM-*Newton* measured to be $T = 7.2^{+0.7}_{-0.6}$ keV; Gioia et al. 2004).

A large number of authors (see Table 5 in Girardi et al. 1996, or Table 2 in Wu et al. 1998 for an exhaustive list of papers on the subject) have attempted to determine the $\sigma_{\rm V} - T_{\rm X}$ using different cluster samples in order to test the dynamical properties of clusters (see among others Girardi et al. 1998; Donahue et al. 1999; Tran et al. 1999; Gioia et al. 1999; Horner et al. 1999; Rosati et al. 2002; Yee & Ellingson 2003; Lubin et al. 2004). This relationship is physically meaningful since both the velocity dispersion of the galaxies and the temperature of the intracluster medium provide a measure of the overall mass of the system. If we characterize the $\sigma_{\rm V} - T_{\rm X}$ relationship as

$$\beta = \frac{\mu m_{\rm p} \sigma_{\rm V}^2}{k T_{\rm gas}}$$

(where μ is the mean molecular weight of the gas, $m_{\rm p}$ is the proton mass and k is the Boltzmann's constant) and if we assume energy equipartition between the galaxies and the gas in the cluster ($\beta = 1$), we obtain a velocity dispersion for RX J1821.6+6827 consistent with the measured one. We derive $\sigma_{\rm V} = 848^{+101}_{-67}$ km s^{-1} from the above $\sigma_{\rm V} - T_{\rm X}$ relation vs. the measured value of $\sigma_{\rm V} = 775^{+182}_{-113}$ km s^{-1}.

Girardi et al. (1996) have derived a best fit relation between the velocity dispersion and the X-ray temperature, with more than 30% reduced scatter with respect to other workers (Edge & Stewart 1991; Lubin & Bahcall 1993; Bird et al. 1995; Wu et al. 1998). Girardi et al. (1996) have taken into account distortions in the velocity fields, asphericity of the cluster or presence of substructures to derive their best fit relation: $\log(\sigma_{\rm V}) = (2.53 \pm 0.04) + (0.61 \pm 0.05) \log(T)$. If we insert the temperature of RX J1821.6+6827 in the above relation, the resulting velocity dispersion value, $\sigma_{\rm V} = 874^{+128}_{-83}$ km s^{-1}, is consistent, even if on the high side, with the measured velocity dispersion.

The temperature of RX J1821.6+6827 is a little lower than predicted from its X-ray luminosity for local $L_X - T_X$ relation. Understanding the evolution of the $L_X - T_X$ relation is important not only to understand the physics behind the formation of galaxy clusters, but also because it provides a link between observations of clusters and derivation of cosmological parameters. There is an extensive literature on the correlation between these two basic and measurable quantities based on *ASCA*, *ROSAT* PSPC and more recently *Chandra* and XMM-*Newton* data (see among other David et al. 1993; Fabian et al. 1994; Mushotzky & Scharf 1997; Markevitch 1998; Sadat et al. 1998; Arnaud & Evrard 1999; Fairley et al. 2000; Borgani et al. 2001; Novicki et al. 2002; Vikhlinin et al. 2002; Lumb et al. 2004). The $L_X - T_X$ relation has been well studied at low redshift. Characterizing the $L_X - T_X$ relation as

$$L_X = L_6 \left(\frac{T}{6\ \mathrm{keV}}\right)^{\alpha}$$

investigators have found for α values ranging from 2.33 to 2.88, all consistent within the errors. There is no consensus yet on the evolution of the $L_X - T_X$ relation with redshift (see among others: Borgani et al. 2001; Novicki et al. 2002; Vikhlinin et al. 2002; Lumb et al. 2004) probably due to the lack of large samples of galaxy clusters at cosmologically significant redshift. Vikhlinin et al. (2002) have detected for the first time an evolutionary trend in the $L_X - T_X$ relation using *Chandra* data for distant clusters. More recently Lumb et al. (2004) have also found an evolutionary trend of the relation using XMM-*Newton* data, albeit using a sample of only 8 clusters in a restricted redshift range ($0.45 < z < 0.62$). On the other hand Ettori et al. (2004) detect only hints of negative evolution in the $L_X - T_X$ using a larger sample of 28 clusters observed by Chandra and in a larger redshift range ($0.4 < z < 1.3$). We assume the parametrization by Arnaud & Evrard (1999) who analyzed a sample of 24 low-z clusters with accurate ASCA temperature measurements and absence of strong cooling flows. Comparing the bolometric luminosity of RX J1821.6+6827 with the Arnaud & Evrard (1999) best fit relation, $\log(L_{\mathrm{BOL,X}}) = (2.88 \pm 0.15)\log(T/6\ \mathrm{keV}) + (45.06 \pm 0.03)$, one would expect for RX J1821.6+6827 a temperature of $6.34^{+0.13}_{-0.35}$ keV that is a little higher, even within the uncertainties, than the best-fit XMM-*Newton* temperature, implying that this cluster may fit better in an evolving $L_X - T_X$ relation. Given the XMM-*Newton* results, RX J1821.6+6827 does not show extreme X-ray luminosity or temperature values.

We can also estimate the mass of RX J1821.6+6827 using the X-ray temperature value. With the assumptions that the mean density in the virialized region is ∼200 times the critical density at the redshift of the cluster and that the cluster is isothermal (Evrard et al. 1996; Donahue et al. 1998), we can use the scaling law method as illustrated in Arnaud & Evrard (1999). From the simulations of Evrard et al. (1996) for the mass-temperature relation one can estimate the virial mass within a radius $r_{200}(T) = 1.85(\frac{T}{10\ \mathrm{keV}})^{1/2}(1+z)^{-3/2}h^{-1}$ Mpc by using the equation

$$M_{\mathrm{vir}} \approx \left(1.45 \times 10^{15}\ h^{-1}\ M_{\odot}\right)(1+z)^{-3/2}\left(\frac{kT_X}{10\ \mathrm{keV}}\right)^{1.5}.$$

From the XMM-*Newton* temperature the virial mass is approximately $M_{\mathrm{vir}} = (1.9^{+0.8}_{-0.4}) \times 10^{14}\ h_{50}^{-1}\ M_{\odot}$ within $r_{200} = 1.04\ h_{50}^{-1}$ Mpc, where the uncertainties on the mass reflect the uncertainties on the temperature.

4. Summary

We have presented observations for the $z = 0.8163$ galaxy cluster RX J1821.6+6827 performed with the instruments on board the XMM-*Newton* satellite, and with the CFHT and Keck-I telescopes. The main result of the paper is to present new optical and X-ray data for the most distant cluster in the NEP survey. Both the temperature and the metal abundance have been left as free parameters in the fitting of the X-ray data with a model. Thus freezing the hydrogen column density to the Galactic value of 5.24×10^{20} atoms cm^{-2} and the redshift to the measured $z = 0.8163$, we obtain a best fit temperature with a thermal MEKAL model of $T = 4.7^{+1.2}_{-0.7}$ keV, while the abundance is unconstrained and can vary in the range $0.28-1.42\ Z_{\odot}$. This X-ray temperature is a little lower than predictions from the cluster X-ray bolometric luminosity $L_{\mathrm{BOL,X}} = 1.35^{+0.08}_{-0.21} \times 10^{45}\ h_{50}^{-2}$ erg s^{-1} ($L_{\mathrm{BOL,X}} = 1.17^{+0.13}_{-0.18} \times 10^{45}\ h_{70}^{-2}$ erg s^{-1} in the concordance cosmology) from the $L_X - T_X$ relation of local clusters published in the literature.

From 18 accepted cluster members we obtain an average redshift $\langle z \rangle = 0.8163 \pm 0.0011$ and a dispersion along the line of sight $\sigma_V = 775^{+182}_{-113}$ km s^{-1}. This measured value is consistent with the velocity dispersion expected from the $\sigma_V - T_X$ relationship obtained from different cluster samples. From the $M - T$ relation we estimate a virial mass for RX J1821.6+6827 within the $r_{200} = 1.04\ h_{50}^{-1}$ Mpc on the assumptions that the mean density in the virialized region is ∼200 times the critical density at the redshift of the cluster and that the cluster is isothermal. The estimated virial mass has a value of $M_{\mathrm{vir}} = 1.9^{+0.8}_{-0.4} \times 10^{14}\ h_{50}^{-1}\ M_{\odot}$ which shows that RX J1821.6+6827 is a massive cluster at high redshift.

The point source to the south, RX J1821.9+6818, identified in the NEP survey as a QSO at $z = 1.692 \pm 0.008$, is well fitted by an absorbed power law with $N_H = 4.1^{+3.1}_{-3.0} \times 10^{20}$ atoms cm^{-2} and a photon index $\Gamma = 1.67 \pm 0.12$ which is typical for this class of objects.

Acknowledgements. I.M.G. would like to thank the hospitality of the Institute for Astronomy of the University of Hawai'i where this paper was written. She also notes that this work was done in spite of the continued efforts by the Italian government to dismantle publicly-funded fundamental research. An anonymous referee made several comments which improved the manuscript. Partial financial support for this work came from the Italian Space Agency ASI (Agenzia Spaziale Italiana) through grant ASI I/R/037/00.

References

Anders, E., & Grevesse, N. 1989, Geochim. Cosmochim. Acta, 53, 197

Arnaud, M., & Evrard, A. E. 1999, MNRAS, 305, 631

Beers, T. C., Flynn, K., & Gebhardt, K. 1990, AJ, 100, 32

Bird, C. M., & Beers, T. C. 1993, AJ, 105, 1596
Bird, C. M., Mushotzky, R. F., & Metzler, C. A. 1995, ApJ, 453, 40
Borgani, S., Rosati, P., Tozzi, P., & Norman, C. 1999, ApJ, 517, 40
Borgani, S., Rosati, P., Tozzi, P., et al. 2001, ApJ, 561, 13
Danese, L., de Zotti, G., & di Tullio, G. 1980, A&A, 82, 322
David, L. P., Slyz, A., Jones, C., et al. 1993, ApJ, 412, 479
Donahue, M., Voit, G. M., Gioia, I., et al. 1998, ApJ, 502, 550
Donahue, M., Voit, G. M., Scharf, C. A., et al. 1999, ApJ, 527, 525
Edge, A. C., & Stewart, G. C. 1991, MNRAS, 252, 414
Eke, V. R., Cole, S., Frenk, C. S., & Patrick Henry, J. 1998, MNRAS, 298, 1145
Elvis, M., Lockman, F. J., & Fassnacht, C. 1994, ApJS, 95, 413
Ettori, S., Tozzi, P., Borgani, S., & Rosati, P. 2004, A&A, 417, 13
Evrard, A. E., Metzler, C. A., & Navarro, J. F. 1996, ApJ, 469, 494
Fabian, A. C., Crawford, C. S., Edge, A. C., & Mushotzky, R. F. 1994, MNRAS, 267, 779
Fairley, B. W., Jones, L. R., Scharf, C., et al. 2000, MNRAS, 315, 669
Gioia, I. M., Henry, J. P., Mullis, C. R., Ebeling, H., & Wolter, A. 1999, AJ, 117, 2608
Gioia, I. M., Henry, J. P., Mullis, C. R., et al. 2001, ApJ, 553, L105
Gioia, I. M., Henry, J. P., Mullis, C. R., et al. 2003, ApJS, 149, 29
Gioia, I. M., Braito, V., Branchesi, M., et al. 2004, A&A, 419, 517
Girardi, M., Fadda, D., Giuricin, G., et al. 1996, ApJ, 457, 61
Girardi, M., Giuricin, G., Mardirossian, F., Mezzetti, M., & Boschin, W. 1998, ApJ, 505, 74
Grevesse, N., & Sauval, A. J. 1998, Space Sci. Rev., 85, 161
Henry, J. P. 2000, ApJ, 534, 565
Henry, J. P. 2004, ArXiv Astrophysics e-prints
Henry, J. P., & Arnaud, K. A. 1991, ApJ, 372, 410
Henry, J. P., Gioia, I. M., Mullis, C. R., et al. 2001, ApJ, 553, L109
Horner, D. J., Mushotzky, R. F., & Scharf, C. A. 1999, ApJ, 520, 78
Jansen, F., Lumb, D., Altieri, B., et al. 2001, A&A, 365, L1
Kollgaard, R. I., Brinkmann, W., Chester, M. M., et al. 1994, ApJS, 93, 145
Le Fevre, O., Crampton, D., Lilly, S. J., Hammer, F., & Tresse, L. 1995, ApJ, 455, 60
Lubin, L. M., & Bahcall, N. A. 1993, ApJ, 415, L17
Lubin, L. M., Mulchaey, J. S., & Postman, M. 2004, ApJ, 601, L9
Lumb, D. H., Bartlett, J. G., Romer, A. K., et al. 2004, ArXiv Astrophysics e-prints
Markevitch, M. 1998, ApJ, 504, 27
Mewe, R., Gronenschild, E. H. B. M., & van den Oord, G. H. J. 1985, A&AS, 62, 197
Mullis, C. R., Henry, J. P., Gioia, I. M., et al. 2001, ApJ, 553, L115
Mullis, C. R., Henry, J. P., Gioia, I. M., et al. 2004, ApJ, in press
Mushotzky, R. F., & Scharf, C. A. 1997, ApJ, 482, L13
Novicki, M. C., Sornig, M., & Henry, J. P. 2002, AJ, 124, 2413
Oke, J. B., Cohen, J. G., Carr, M., et al. 1995, PASP, 107, 375
Oukbir, J., & Blanchard, A. 1992, A&A, 262, L21
Oukbir, J., & Blanchard, A. 1997, A&A, 317, 1
Peacock, J. A. 1999, Cosmological physics (Cambridge, UK: Cambridge University Press)
Peebles, P. J. E. 1993, Principles of physical cosmology, Princeton Series in Physics (Princeton, NJ: Princeton University Press)
Rosati, P., Borgani, S., & Norman, C. 2002, ARA&A, 40, 539
Rosati, P., Tozzi, P., Ettori, S., et al. 2004, AJ, 127, 230
Sadat, R., Blanchard, A., & Oukbir, J. 1998, A&A, 329, 21
Strüder, L., Briel, U., Dennerl, K., et al. 2001, A&A, 365, L18
Tran, K. H., Kelson, D. D., van Dokkum, P., et al. 1999, ApJ, 522, 39
Turner, M. J. L., Abbey, A., Arnaud, M., et al. 2001, A&A, 365, L27
van Dokkum, P. G., Franx, M., Fabricant, D., Illingworth, G. D., & Kelson, D. D. 2000, ApJ, 541, 95
Vikhlinin, A., VanSpeybroeck, L., Markevitch, M., Forman, W. R., & Grego, L. 2002, ApJ, 578, L107
Vikhlinin, A., Voevodkin, A., Mullis, C. R., et al. 2003, ApJ, 590, 15
Voges, W., Henry, J. P., Briel, U. G., et al. 2001, ApJ, 553, L119
Wu, X., Fang, L., & Xu, W. 1998, A&A, 338, 813
Yee, H. K. C., & Ellingson, E. 2003, ApJ, 585, 215